Carbohydrate Polymers 98 (2013) 1272–1280

Contents lists available at ScienceDirect

Carbohydrate Polymers

journal homepage: www.elsevier.com/locate/carbpol

Xyloglucan-based diblock co-oligomer: Synthesis, self-assembly and steric stabilization of proteins

Cony Gauche[a,b], Valdir Soldi[b], Sébastien Fort[a], Redouane Borsali[a], Sami Halila[a,*]

[a] Centre de Recherches sur les Macromolécules Végétales (CERMAV-CNRS), Université Joseph Fourier (UJF), Institut de Chimie Moléculaire de Grenoble (ICMG-FR 2607 CNRS), PolyNat Carnot Institute, Arcane LabEx, BP 53, F-38041 Grenoble Cedex 9, France
[b] Department of Chemistry, Universidade Federal de Santa Catarina, 88040-900, Florianópolis, Brazil

ARTICLE INFO

Article history:
Received 28 June 2013
Received in revised form 25 July 2013
Accepted 28 July 2013
Available online 6 August 2013

Keywords:
Xyloglucan oligosaccharides
Click reaction
Amphiphilic block co-oligomer
Self-assembly
Micelles
Protein stabilization

ABSTRACT

We propose a novel plant-based amphiphilic diblock co-oligomers (BCO) surfactant containing only carbohydrate segments and examine its potential as a biosourced stabilizer. The synthesis of an amphiphilic xyloglucan-based BCO, composed of a hydrophilic xyloglucan oligosaccharide (XGO) block "clicked" to a hydrophobic peracetylated XGO is described. Dynamic light scattering experiments correlated with transmission electron microscopy observations showed that this new class of amphiphilic BCO self-assembles in water to form spherical micelles with a hydrodynamic diameter of 22 nm. Preliminary studies indicate that the XGO-based BCO sterically stabilizes gliadin and zein nanoparticle suspensions. The stabilization results were compared to those using pluronic F-68, a commercial surfactant. For gliadin nanoparticles, both surfactants result in essentially the same morphology and polydispersity. However, for the zein nanoparticles, the XGO-based BCO stabilizer gave lower polydispersity.

1. Introduction

Colloidal drug carrier systems have gained increasing interest for the possibility of drug targeting by modifying the eventual body distribution of the drugs as well as their improvement of the cellular uptake (Schafer et al., 1992). In this respect, the search for nanoparticulate systems aiming at the loading of poorly water soluble active agents with pronounced toxic side effects has been the focus of intensive research for some years (Adair, Parette, Atinoglu, & Kester, 2010; Ambade, Savariar, & Thayumanavan, 2005; Kataoka, Harada, & Nagasaki, 2001). Among various nanoscale delivery vehicles, nanoparticle protein systems offers advantageous potential solutions. These include increasing the drug intratumor concentration (Hawkins, Soon-Shiong, & Desai, 2008), and high specificity and low immunological responses. Additionally, therapeutic proteins have been widely used to treat diabetes, hepatitis, inflammation and other diseases (Leader, Baca, & Golan, 2008). Colloidal systems made from gliadin and zein are promising nanocarriers extracted from gluten of wheat and maize, respectively, and usually labeled as "vegetable protein" (Ezpeleta et al., 1996). Gliadin, thanks to its versatile biodegradability, biocompatibility and natural origin (Jahanshahi & Babaei, 2008) is considered to be a suitable biopolymer for the preparation of nanoparticles, with interesting adsorption affinity with intestinal mucosal (Arangoa et al., 2000; Arangoa, Campanero, & Irache, 2004; Ezpeleta et al., 1999). On the other hand, zein, a proline-rich, water insoluble corn storage protein, has been studied as a potential biomaterial for the development of colloidal delivery systems (Liu, Sun, Wang, Zhang, & Wang, 2005; Mastromatteo, Barbuzzi, Conte, & Del Nobile, 2009; Parris, Cooke, Hicks, 2005; Torres-Giner, Gimenez, & Lagaron, 2008; Zhong & Jin, 2009a). Classified as "Generally Recognized as Safe (GRAS)" by the US Food and Drug Administration, zein shows a good biodegradability (Wang et al., 2007) and in vivo cell compatibility (Dong, Sun, & Wang, 2004; Liu et al., 2005; Wang, Lin, Liu, Sheng, & Wang, 2005).

However, most of peptides and proteins are quite unstable, prone to denaturation and aggregation (Yadav, Kumari, & Yadav, 2011). The simplest and most common method to overcome these limitations is to change the nature of the environment surrounding the protein by adjusting solution conditions such as pH, or by adding stabilizers. Nonionic surfactants can be used to protect and stabilize proteins against surface-induced aggregation, either by binding to the proteins and preventing protein-protein associations, or by saturating the interface and thus minimizing adsorption and subsequent conformational changes (Lee, McAuley, Schilke, & McGuire, 2011). Among them, nonionic block copolymer surfactants are a family class widely used in pharmaceutical applications (Schmolka, 1991). Compared to classical surfactants, amphiphilic block copolymers have the advantage that their ordering properties can be nearly continuously tuned by adjusting solvent composition, molecular weight, or copolymer architecture. Moreover, their

* Corresponding author. Tel.: +33 0 476037666; fax: +33 0 476547203.
E-mail address: sami.halila@cermav.cnrs.fr (S. Halila).

0144-8617/$ – see front matter © 2013 Elsevier Ltd. All rights reserved.
http://dx.doi.org/10.1016/j.carbpol.2013.07.064

self-organization in solution usually leads to various structural features, even at low concentrations. Considering the wide range of pharmaceutical applications of nonionic block copolymer surfactants, their toxicity with respect to chronic uptake must be considered. For example, results obtained by Magnusson, Olsson, and Nyberg (1986) showed that Pluronic F-68, belonging to the poloxamers' family, is able to induce phospholipidosis in rats, as well as pulmonary foam cells at dose levels above 500 mg/kg and slight focal degenerative changes in the proximal tubules of the kidneys above 100 mg/kg. Moreover, the slow environmental degradability of the major types of water-soluble block copolymers, e.g., the pluronic-based compounds, has become a major obstacle for their industrial development.

Thus, motivated by industrial requirements for nontoxic, biocompatible and biodegradable stabilizers, the use of carbohydrates as polar head groups in amphiphilic block copolymer surfactants has been studied (Greffe, Bessueille, Bulone, & Brumer, 2005; Halila et al., 2008; Nowicki, Sokolowski, & Reksa, 2011; Kida et al., 2004). Carbohydrates are biopolymers produced annually in massive amounts by a broad variety of plants and microorganisms. Because they possess great structural and superstructural diversity, carbohydrates serve important biological functions, such as in cellular interaction and communication. Reference works have demonstrated that polysaccharide-decorated materials for biomedical applications usually exhibit enhanced absorption, permeability and bioadhesion properties, favoring biocompatibility and molecular recognition processes (Barsett et al., 2005)

Recently, we have successfully developed a fully oligosaccharide-based amphiphilic block co-oligomers (BCO) in which the hydrophilic block consisted of a free maltoheptaosyl derivative clicked to a hydrophobic block composed of a peracetylated maltoheptaosyl derivative, referred to as Mal_7-*b*-$AcMal_7$ (Modolon et al., 2012). Maltoheptaose is a linear α-(1,4) glucan of seven glucosyl units obtained from the ring-opening of *β*-cyclodextrin by acid hydrolysis. Mal_7-*b*-$AcMal_7$ self-assembled in spherical nanoparticles in water with an average diameter of 56 nm. This type of fully oligosaccharide-based amphiphilic BCO could find interest as a low-molecular weight block copolymer surfactant stabilizing proteins to prevent their aggregation.

To improve the later system and for practical and economic reasons, we propose a new co-oligomer synthesized exclusively from tamarind seeds xyloglucan oligosaccharides (XGOs). In fact, XGOs are easily obtained from controlled enzymatic depolymerization of commercially available tamarind seeds xyloglucan – the most abundant hemicellulose found in plant primary cell wall (Carpita & Gibeaut, 1993) – using commercial cellulases (endo-*β*-1,4-glucanase) (Greffe et al., 2005; Halila et al., 2008). Structurally, tamarind seeds xyloglucans are based on a linear β(1→4)-glucan backbone, regularly branched with α(1→6)-xylosyl units, that in turn can be further substituted with β(1→2)-galactosyl units (Fig. 1).

The goal of this work is to design a new class of XGO-based linear amphiphilic BCO and to evaluate its stabilizing effects on gliadin and zein. To reach these objectives we have functionalized each reducing-end of the blocks by regioselective modification using a microwave-assisted reductive amination and then, we made one of blocks hydrophobic through ester protecting groups of hydroxyl groups. Finally, the blocks were linked by Cu(I)-catalyzed azide-alkyne cycloaddition "click chemistry" (CuAAC) (Rostovtsev, Green, Fokin, & Sharpless, 2002; Tornoe, Christensen, Meldal, 2002). The present approach opens up a new class of amphiphilic block copolymer surfactants based on vegetal raw materials that provide steric stabilization, preventing the aggregation of gliadin and zein nanoparticles in aqueous solution.

2. Experimental

2.1. Materials

Tamarind seed xyloglucan (XG, purity ≥ 95%) was kindly supplied from Dainippon Pharmaceutical Co., Ltd (Osaka, Japan). Sodium cyanoborohydride, dry dimethylformamide, propargyl bromide, gliadin and zein were purchased from Sigma-Aldrich (St. Louis, MO). Methanol, ethanol, acetic acid, acetic anhydride, ethyl acetate, hydrochloric acid, pyridine and acetonitrile were purchased from SDS with analytical grade quality (Carlo Erba). Propargylamine 99% was purchased from ACROS Organics and 4-dimethylaminopyridine from Lancaster Synthesis Inc. They were all used as received. Water was purified by a Milli-Q water purification system (Billerica, MA, USA). 2-Azidoethylamine and $CuI{\cdot}P(OEt)_3$ were prepared according to the literature (Efthymiou, Huynh, Oentoro, Peel, & Desaulniers, 2012; Ziegler, Fowler, Rodgers, & Wester, 1987).

2.2. Instrumentation

Reactions were followed by thin layer chromatography (TLC) on silica gel $60F_{254}$ (E. Merck) by charring with sulfuric acid solution (H_2SO_4/MeOH/H_2O, 3:45:45). Flash-column chromatography was performed on silica gel 60 (40–63 μm, E. Merck) or C18 (Grace Reveleris® Silica Flash Cartridges, 12 g). The ^1H NMR and ^{13}C NMR spectra were recorded at 298 K using a 400 MHz Bruker Avance DRX400. The solvent residual peaks of D_2O, $(CD_3)_2SO$ and $CDCl_3$ were used as internal standards, at 4.79 ppm, 2.50 ppm and 7.26 ppm, respectively. Infrared (IR) spectra were recorded using a Perkin-Elmer Spectrum RXI FTIR Spectrometer. MALDI-TOF measurements were performed on a Bruker Daltonics Autoflex apparatus. Fluorescence spectra were recorded on a HITACHI F4500 spectrofluorimeter equipped with a thermostated cell holder set at 25.0 °C. The static and dynamic light scattering experiments were carried out using an ALV setup. Transmission electron microscopy (TEM) experiments were carried out using a CM220 Philips microscope.

2.3. Synthesis

XGO_N_3 (2). To a suspension of XGOs (1) (1.0 g, 0.78 mmol) (made up of a mixture of hepta-, octa-, and nona-saccharides in the ratio 0.15:0.35:0.50, respectively) in water/methanol (8 mL; 1:1, v/v) acidified with acetic acid (until pH 5.0) were added 2 Eq. $NaBH_3CN$ (98 mg; 1.56 mmol) and 2 Eq. 2-azidoethylamine (98 mg; 1.56 mmol). The reaction mixture was heated in a microwave system at 80 °C for 2 h. Precipitation in ethanol (80 mL) was carried out and the suspension was centrifuged (8000 rpm for 10 min at 4 °C). The supernatant was removed and this procedure was repeated once. The residue was dissolved in water, lyophilized and purified by automated flash chromatography on C18 reversed phase column (H_2O:MeOH, 0 to 80% in MeOH) to provide (2) as white solid, 0.703 g (66% yield). IR (KBr): ν = 3300 (O—H, sugars), 2894 (C—H, sugars), 2100 (N_3, azide) cm^{-1}; ^1H NMR (400 MHz, D_2O): δ = 5.2 (m, H-1 $Xyl^{II,\ III}$), 4.97–4.96 (m, H-1 Xyl^{IV}), 4.62–4.50 (m, H-1 $Glc^{II–IV}$, $Gal^{II,\ III}$), 4.04–2.88 (m, H-2 to H-6 $Glc^{II–IV}$ and $Gal^{II–III}$, H-2 to H-5 $Xyl^{II–IV}$ H-1 Glc^{I}-itol, NCH2), 1.93 ppm (s, CH_2N_3); MALDI-TOF: calcd for (nona-saccharide) $[M+Na]^+$ *m/z* 1479.52, found 1479.44, calcd for (octa-saccharide) $[M+Na]^+$ *m/z* 1317.47, found 1317.39, calcd for (hepta-saccharide) $[M+Na]^+$ *m/z* 1155.41, found 1155.34.

XGO_Propargyl (3). To a suspension of XGOs (1.0 g, 0.79 mmol) (1) (made up of a mixture of hepta-, octa-, and nona-saccharides in the ratio 0.15:0.35:0.50, respectively) in water/methanol (8 mL; 1:1, v/v) acidified with acetic acid (until pH 5.0) were added 2 Eq. $NaBH_3CN$ (98 mg; 1.56 mmol) and 2 Eq. propargylamine (86.3 mg;

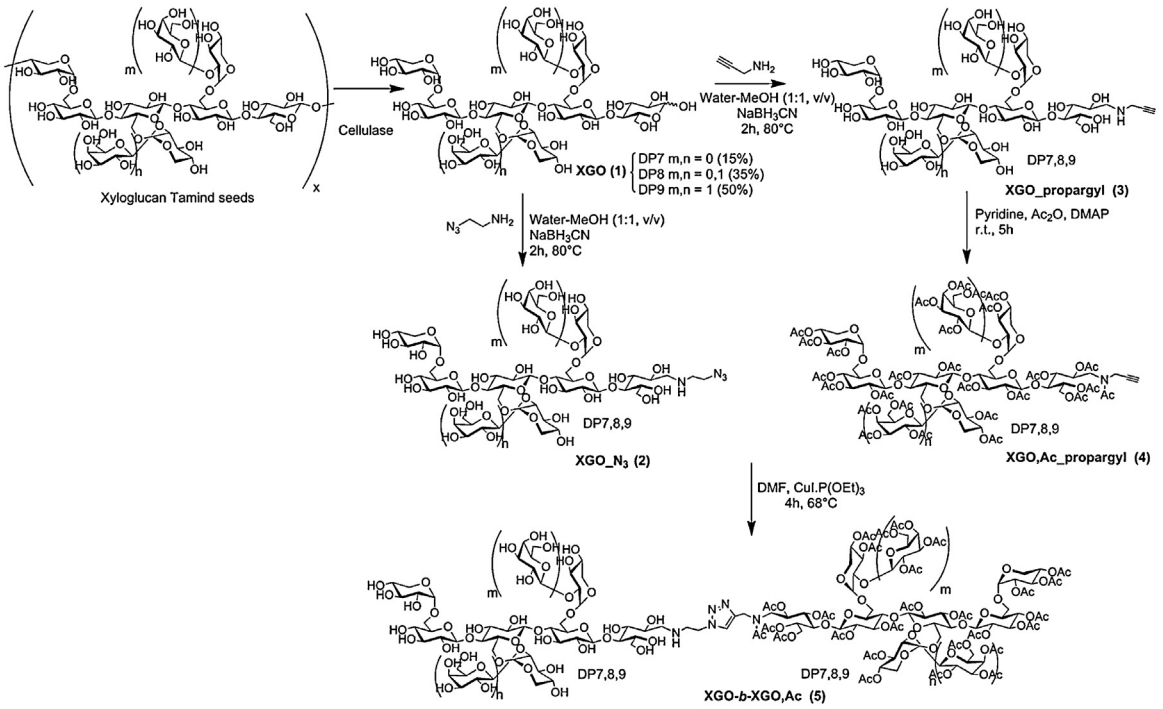

Fig. 1. Synthetic route to XGO-*b*-XGO,Ac block co-oligomer.

1.56 mmol). The reaction mixture was heated in a microwave system, at 80 °C for 2 h. Precipitation in ethanol (80 mL) was carried out and the suspension was centrifuged (8000 rpm for 10 min at 4 °C). The supernatant was removed and this procedure was repeated once. The residue was dissolved in water, lyophilized and purified by automated flash chromatography on a C18 reversed phase column (H_2O:MeOH, 0 to 80% in MeOH) to provide (3) as a white solid, 0.497 g (58% yield). IR (KBr): ν = 3398–3368 (O—H, sugars), 2925 (C—H, sugars), 2115 (C≡C, alkyne) cm^{-1}; ^1H NMR (400 MHz, D_2O): δ = 5.18–5.19 (m, H-1 $Xyl^{II,\ III}$), 4.95–4.97 (m, H-1 Xyl^{IV}), 4.53–5.59 (m, H-2 to H-6 $Glc^{II–IV}$ and $Gal^{II–III}$, H-2 to H-5 $Xyl^{II–IV}$, H-1 Glc^{I}-itol, NCH_2), 2.68 and 2.81–2.92 ppm (m, C≡CH); MALDI-TOF: calcd for (nona-saccharide) $[M + Na]^+$ *m/z* 1448.50, found 1448.52, calcd for (octa-saccharide) $[M + Na]^+$ *m/z* 1286.45, found 1286.43, calcd for (hepta-saccharide) $[M + Na]^+$ *m/z* 1124.40, found 1124.36.

XGO, Ac_Propargyl (4). A solution of XGO-propargyl (0.5 g, 0.35 mmol) (3) in pyridine (50 mL), Ac_2O (20 mL) and DMAP was stirred at room temperature up to the complete disappearance of the starting material, followed by TLC (eluent: 7:3, acetonitrile-water). Methanol was added and then the solvent was evaporated under reduced pressure. The residue was dissolved in ethyl acetate (200 mL) and successively washed with HCl 1 N (200 mL) and water (200 mL). The organic layer was dried on Na_2SO_4 and concentrated to dryness in vacuo with a rotary evaporator. Purification by column chromatography (SiO_2, Ethyl acetate) afforded (4) as a yellowish powder, 0.725 g (81% yield). IR: ν = 2115 (C—C, alkyne), 1751 (C=O, ester) cm^{-1}; ^1H NMR (400 MHz, $CDCl_3$): δ = 5.39–3.65 (m, H-1 $Xyl^{II,\ III,IV}$, H-2 to H-6 $Glc^{II–IV}$ and $Gal^{II–III}$, H-2 to H-5 $Xyl^{II–IV}$, H-1 Glc^{I}-itol, NCH_2), 2.53, 2.32–2.34 and 2.24 (m, C≡CH), 1.95–2.19 (m, $COCH_3$); MALDI-TOF: calcd for (nona-saccharide) $[M + Na]^+$ *m/z* 2582.79, found 2582.63, calcd for (octa-saccharide) $[M + Na]^+$ *m/z* 2294.70, found 2294.61.

XGO-b-XGO,Ac (5). To a solution of XGO, Ac_propargyl (0.1 g, 0.039 mmol) (4) and 1 Eq. XGO_N_3 (53.2 mg, 0.039 mmol) (2) in dry dimethylformamide (1 mL) was added 0.5 Eq. CuI·$P(OEt)_3$ (6.9 mg, 0.0195 mmol) under argon atmosphere. The reaction mixture was stirred at 68 °C for 3 h until TLC showed no change of the starting material consumption. Methanol was added and the reaction mixture was evaporated under reduced pressure in the presence of silica. The crude solid was purified by flash column chromatography on silica gel (eluent: 8:2, acetonitrile-water and 7:3, acetonitrile-water) to yield the XGO-*b*-XGO,Ac (5) as a white solid, 0.169 g (95% yield). IR (KBr): ν = 3455–3395 (OH, sugars), 2939–2894 (C—H, sugars), 1751 (C=O, ester) cm^{-1}; ^1H NMR (400 MHz, $(CD_3)_2SO$): δ = 8.02, 7.94 and 7.83 (3x s, H-5 triazole), 5.34–2.48 (m, H-1 $Xyl^{II,\ III,IV}$, H-2 to H-6 $Glc^{II–IV}$ and $Gal^{II–III}$, H-2 to H-5 $Xyl^{II–IV}$, H-1 Glc^{I}-itol, NCH_2), 2.14–1.88 ppm (m, CH_3 (OAc)); MALDI-TOF: calcd for (DP9-*b*-DP9,Ac) $[M + Na]^+$ *m/z* 4039.31, found 4039.04, calcd for (DP8-*b*-DP9,Ac) $[M + Na]^+$ *m/z* 3877.25, found 3877.04, calcd for (DP9-*b*-DP8,Ac) $[M + Na]^+$ *m/z* 3751.21, found 3751.04, calcd for (DP8-*b*-DP8,Ac) $[M + Na]^+$ *m/z* 3589.17, found 3589.02.

2.4. Sample preparation and experimental setup

2.4.1. Static and dynamic light scattering measurements

The aqueous solutions of XGO-*b*-XGO,Ac 5 (1.0, 3.0, 5.0 mg mL^{-1}) were stirred overnight at 40 °C, then filtered through 0.45 μm MILLIPORE Millex LCR filters. Scattering measurements were performed using an ALV-CGS 8F S/N 069 laser goniometer, which consists of a 22 mW HeNe linear polarized laser operating at a wavelength of 632.8 nm, an ALV-5004 multiple τ digital correlator with 125 ns initial sampling time. The samples were kept at a constant temperature of 25.0 ± 0.1 °C during all the experiments. The measurements were recorded at an angle of 90°. The aqueous solutions were put in 10 mm diameter glass cells. The minimum sample volume required for the experiment was 1 mL. Data were collected using the digital ALV Correlator Control software, and the counting time for each sample was 300 s.

The aqueous solutions of XGO-*b*-XGO,Ac 5 (3.0 mg mL^{-1}) micelles were also analyzed by Nanoparticle Tracking Analysis (NTA) using a digital microscope LM10 System (NanoSight, Salisbury, UK). Video images of particle movement under Brownian motion were analyzed by the NTA analytical software version 2.1.

The measurements were made at room temperature and the video clip was captured over 60 s. NTA video obtained for XGO-*b*-XGO,Ac micelles is available as supplementary data.

2.4.2. Fluorescence measurements

The critical micelle concentration (CMC) for XGO-*b*-XGO,Ac 5 was determined by fluorescence spectroscopic analysis, using pyrene as a hydrophobic fluorescent probe. The steady-state fluorescence emission spectra of pyrene were recorded on a Hitachi F4500 Spectrofluorimeter equipped with a thermostated cell holder at 25.0 ± 0.1 °C, and the samples were continuously stirred in a 10 mm path length quartz cell. The concentration of the probe was fixed at 1.0×10^{-6} mol L^{-1} and the sample concentration range was from 3×10^{-3} mg mL^{-1} to 1.2 mg mL^{-1}. The probe was excited at 336 nm, and the emission spectrum was collected in the range 360–450 nm. Both slit width settings of excitation and emission monochromators were adjusted to 2.5 nm. The intensity of the first (I_{m1}) vibronic band over the third (I_{m3}), I_{m1}/I_{m3} ratio located at 372.8 and 384 nm in the emission spectrum of monomeric pyrene provides an estimation of the polarity in a pyrene environment.

2.4.3. Transmission Electron Microscopy (TEM) measurements

Transmission electron microscopy (TEM) images were recorded on a JEM-1011 microscope operating at 80 kV. The samples were analyzed using the same concentrations as in the light scattering experiments. Solutions (4 μL) were dropped on a copper-coated grid, which was made hydrophilic by glow discharge treatment, and then dried at room temperature.

2.4.4. Protein nanoparticles

To evaluate the surfactant ability of the new amphiphilic block co-oligomer synthesized in this work, we prepared gliadin and zein nanoparticles in aqueous solutions. Protein nanoparticles were prepared by a liquid-liquid dispersion method as suggested by Zhong and Jin (2009b) with slight modifications. First, protein solutions were prepared by dissolving gliadin in ethanol 62% (Duclairoir, Nakache, Marchais, & Orecchioni, 1998) or zein in ethanol 85% (Zhong & Jin, 2009b) (5 g L^{-1}). This solution was filtered through 0.45 μm MILLIPORE Milles LCR filters and then poured into magnetically stirred (1000 rpm) solution containing Pluronic F-68 or the amphiphilic XGO-*b*-XGOAc 5, as stabilizers, at different concentrations.

Scattering measurements (DLS/SLS) were performed using an ALV laser goniometer to determine the nanoparticle sizes, and TEM measurements were performed to determine the nanoparticle shapes.

2.4.5. Statistical analysis

Statistical analysis of the average values obtained from diameter size and polydispersity index were calculated by Analysis of Variance (ANOVA) and the Tukey test was applied when a 5% difference in the level of these values was verified. All analyses were evaluated by the STATISTICA Software version 10.0 (StatSoft, Inc., 1984-2011, Tulsa, OK, USA).

3. Results and discussion

3.1. Synthesis and structural characterization of XGO-b-XGO,Ac

Xyloglucan oligosaccharides (XGOs) are the saccharidic blocks constituting the amphiphilic block co-oligomer (Fig. 1). They were obtained by enzymatic digestion of tamarind seed xyloglucan powder with commercial cellulases (Halila et al., 2008; Hisamatsu, York, Darvill, & Albersheim, 1992). In order to build the XGO-*b*-XGO,Ac diblock by means of click chemistry, we chose to introduce the azide function on free XGOs, and the alkyne function on the hydrophobic XGOs.

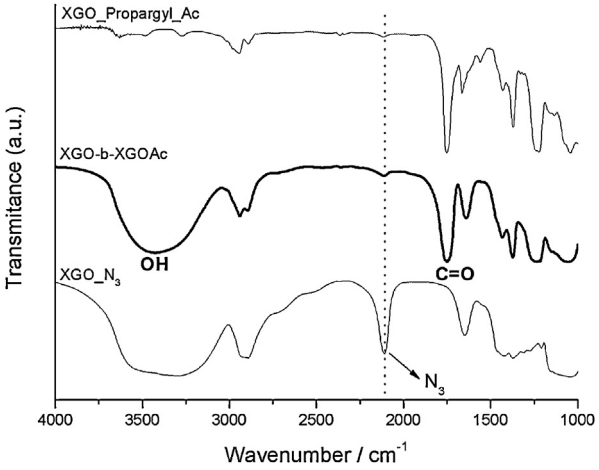

Fig. 2. FTIR spectra of XGO,Ac_propargyl, XGO-*b*-XGO,Ac and XGO_N_3.

First, free oligosaccharides 1 were chemoselectively functionalized with 2-azidoethylamine linker by microwave-assisted reductive amination at 80 °C for 2 h. The reaction involves condensation of the ring-opened (carbonyl) form of the reducing-end of the oligosaccharides with the amine counterpart. The resulting Schiff base intermediate is relatively unstable (Dalpathado, Jiang, Kater, & Desaire, 2005) and is quickly reduced to the corresponding secondary amine by action of the reducing agent, $NaBH_3CN$. XGO_N_3 2 was isolated by simple precipitation in ethanol with 66% yield. The chemical structure of 2 was confirmed by ^{1}H-NMR, FT-IR and mass spectrometry. The presence of the terminal azido group was confirmed by FT-IR analysis with the stretching frequency around 2100 cm^{-1}.

Second, following the same procedure, the XGOs were functionalized with a propargylamine linker to give XGO_propargyl 3 with 58% yield. Peracetylation of XGO_propargyl with acetic anhydride and DMAP in pyridine provided the hydrophobic block, XGO,Ac_propargyl 4. As previously, the chemical structure of 4 was confirmed by ^{1}H-NMR, FT-IR and mass spectrometry.

In spite of moderate yield, around 60%, the microwave-assisted reductive amination enables formation of both blocks in less than 1 day and with the ensuing purification process using a single step ethanolic precipitation, the reaction could be carried out on a large scale.

We then performed the "click" reaction in dry DMF between XGO_N_3 2 and XGO,Ac_propargyl 4 using CuI·$P(OEt)_3$ as the catalyst under argon atmosphere at 60 °C for 4 h then for 48 h at room temperature (Fig. 1). The reaction was monitored by TLC and the product was isolated by flash chromatography on silica gel, using acetonitrile/water as the eluent, giving the diblock XGO-*b*-XGO,Ac 5 with 95% yield. FT-IR analysis of the purified product showed the complete disappearance of transmittance due to the azide group (2100 cm^{-1}) (Fig. 2), indicating that there is no unreacted XGO_N_3 2 in the XGO-*b*-XGO,Ac 5. Moreover, the ^{1}H NMR spectra showed resonances at the range of 7.85–8.0 ppm, corresponding to the olefinic proton associated with the 1,4-disubstituited 1,2,3-triazole isomer moiety in accordance with assigned structures (Fig. 3). In addition, the characteristic signals due to the protons of the free xyloglucan, and the protons of the acetylated xyloglucan were also observed. MALDI-TOF mass spectrometry providing confirmation of the successful end-to-end coupling with the presence of different combination of molecular ions produced from the click reaction between XGO_N3 (DP7,8,9) 2 and XGO,Ac_propargyl (DP7,8,9) 4.

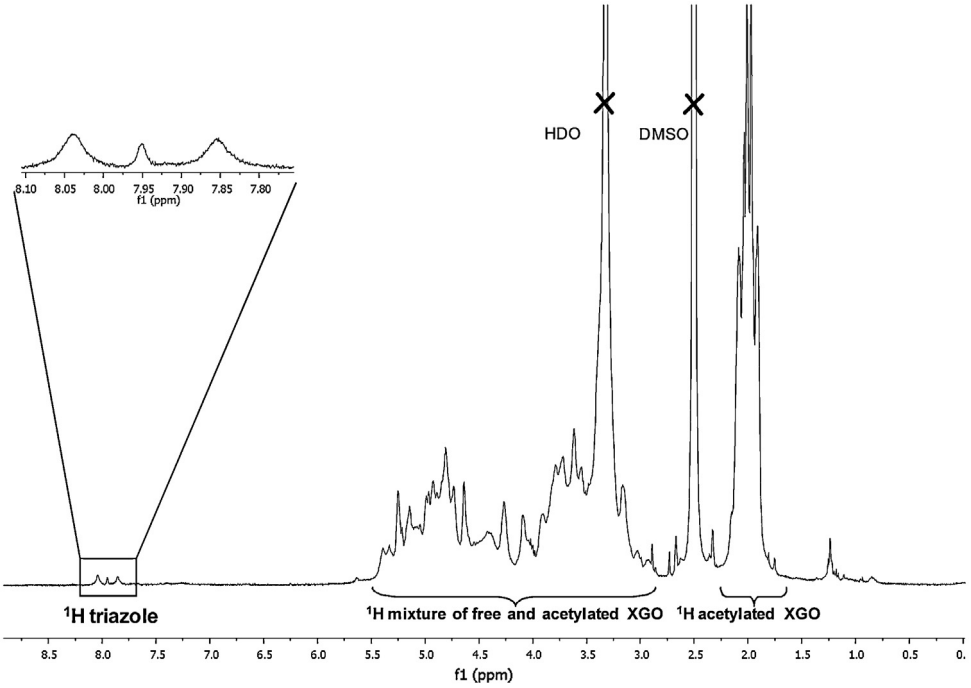

Fig. 3. ^{1}H NMR spectrum of XGO-*b*-XGO,Ac.

3.2. Self-assembly of amphiphilic XGO-b-XGO,Ac 5 in water

The critical micelle concentration (CMC) is one of the basic parameters for characterizing micellization (Kwon et al., 1993). The CMC is the polymer concentration, above which the formation of micelles occurs. The CMC of XGO-*b*-XGO,Ac 5 was determined by a fluorescence technique using pyrene as a probe. Pyrene has been extensively used to monitor the CMC of a variety of aggregation processes.

The XGO-based diblocks showed a CMC value of 0.04 mg mL^{-1} (1.10^{-5} mol L^{-1}) (Fig. 4), lower than 0.1 mg mL^{-1} (3.10^{-5} mol L^{-1}) value obtained for Mal_7-"click"-$AcMal_7$ (Modolon et al., 2012), but near the range reported for a low molecular weight nonionic surfactant (Zhang, Zhang, & Somasundaran, 2004). The CMC difference can be explained due to the molecular shape and lower solubility in water of branched peracetylated xyloglucan oligosaccharides, compared to the linear structure of maltoheptaose. If the hydrophilic block is kept constant, an increase in the molecular weight of the hydrophobic block will decrease CMC value, while a lesser effect is observed when we change the molecular weight of corona-forming block (Allen, Maysinger, & Eisenberg, 1999). Compared to *N*-alkyl XGO aminoalditols (XGO-C*n*) surfactants (Greffe et al., 2005), the CMC value of XGO-*b*-XGO,Ac is roughly equivalent to a XGO-C16 (C16 means 16 carbon atoms constituting the fatty acid main chain). This means that, in terms of the CMC, a peracetylated XGO can be considered as a C-16 alkyl chain.

Moreover, the small CMC value obtained for the XGO-*b*-XGO,Ac is promising in the field of drug delivery vehicles, due to the probable stability of the micelles upon dilution in the bloodstream. Thus, at same concentration, XGO-*b*-XGO,Ac micelles might show higher stability upon dilution compared to Pluronic F68 which has a CMC value one hundred times higher (ca. 4 mg mL^{-1}) (Nakashima, Anzai, & Fujimoto, 1994).

The self-assembly in solution of amphiphilic XGO-*b*-XGO,Ac 5 was evaluated through scattering measurements by direct dilution in deionized water. Nanoparticles prepared at a concentration of 3.0 mg mL^{-1} were detected at 90° scattering angle by DLS. The results in a number distribution (Fig. 5B) that shows that the diblock self-organizes in water to form, predominantly, micelles with a hydrodynamic diameter of about 22 nm. Because large particles scatter light much more than small particles, the DLS weight distribution (Fig. 5A) showed mainly bigger aggregates whose size was 150 nm in diameter.

The concentration effect on the micelle size was evaluated at a range from 1 to 10 mg mL^{-1}. The results showed a slight variation (19 to 22 nm in diameter) with the concentration increase, indicating that micelles size were stable and homogeneous in the concentration range studied.

To check the micelle morphology and size, we performed TEM measurements. The TEM image of XGO-*b*-XGO,Ac 5 in water at 3.0 mg mL^{-1} (Fig. 6) indicated that the formed micelles have spherical morphology and an average diameter of about 25 nm. The image analysis showed that single micelles were the most common, in agreement with number diameter distribution by DLS.

Following the structural characterization and physico-chemical studies of the XGO-*b*-XGO,Ac 5 micelles, we investigated their protein-stabilizing properties.

3.3. Protein nanoparticles

We compared the stabilizing properties of XGO-*b*-XGO,Ac 5 with F68-pluronic on gliadin and zein nanoparticles in a set of preliminary studies. The method used to prepare protein nanoparticles consisted on a two-step desolvation characterized by the adding of a good solvent phase (ethanol:water) to a non-solvent phase (water) (Ezpeleta et al., 1996; Zhong & Jin, 2009b) and the subsequent stabilization by a surfactant. These stabilizers (surfactant and/or polymer) should act as an energy barrier around the particles, thus preventing aggregation (Tadros, 2005). For the BCO, the hydrophobic block XGO,Ac of the non-ionic amphiphilic BCO should interact through hydrophobic bonding to the nonpolar parts on the globular proteins surface.

The DLS results (Table 1) showed that the gliadin nanoparticle diameters, around 400 nm, were not significantly ($p > 0.05$) influenced either by the utilization of the surfactants or by concentration changes. The same behavior was observed for the polydispersity

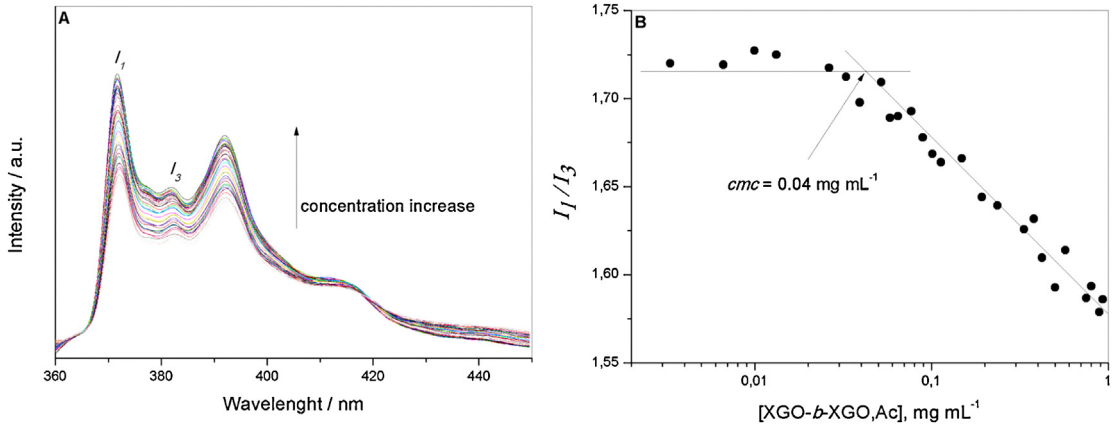

Fig. 4. Pyrene fluorescence emission spectra and the corresponding variation in the I_1/I_3 ratio as a function of XGO-*b*-XGO,Ac concentration ([pyrene] = 6.10^{-7} mol L^{-1}).

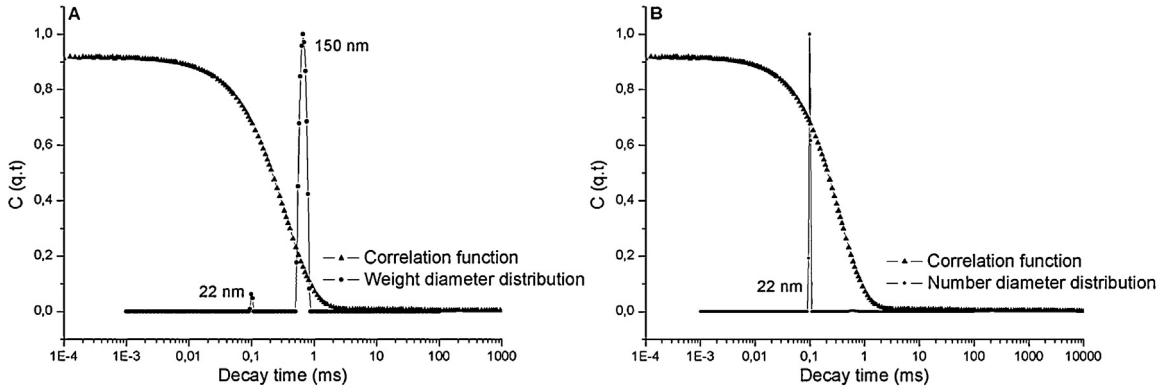

Fig. 5. Dynamic light scattering autocorrelation function, weight diameter distribution (5A) and number diameter distribution (5B) of XGO-*b*-XGO,Ac in water ([XGO-*b*-XGO,Ac] = 3 mg mL^{-1}, scattering angle = 90°, temperature = 25 °C).

index (PDI) of gliadin nanoparticles, where the nature of surfactants and the concentration used did not show differences between values at a significance level of 5% (ANOVA for Analysis Of VAriance).

We observed in TEM as shown in Fig. 7 (left) that the gliadin nanoparticles prepared with 0.05% Pluronic or XGO-*b*-XGOAc 5 exhibited the same morphology like solid spheres. Without stabilizer, the gliadin nanoparticles in solution have irregular spherical shapes with packed aggregates of apparent diameter similar to those obtained from DLS, i.e., around 400–500 nm. With the addition of 0.05% XGO-*b*-XGO,Ac 5 or F68-pluronic, well-shaped spherical gliadin nanoparticles of ca. 400 nm-diameter were obtained and the magnified pictures showed a surrounded thick layer of surfactant that stabilized the hydrophobic gliadin core. In Fig. 7C, we observe small aggregates of low-density which could correspond to other gliadin nanoparticules stabilized by a thin layer of XGO-*b*-XGO,Ac 5. This new family of small aggregates was not observed by DLS, probably because the large aggregates have much stronger scattering signals than the smaller ones.

In the case of the zein nanoparticles, a significant ($p < 0.05$) differences were observed when the nanoparticles were prepared with different surfactants ($p = 0.000$), but the concentration variation ($p > 0.05$) did not affect the nanoparticle size (Table 1). The use

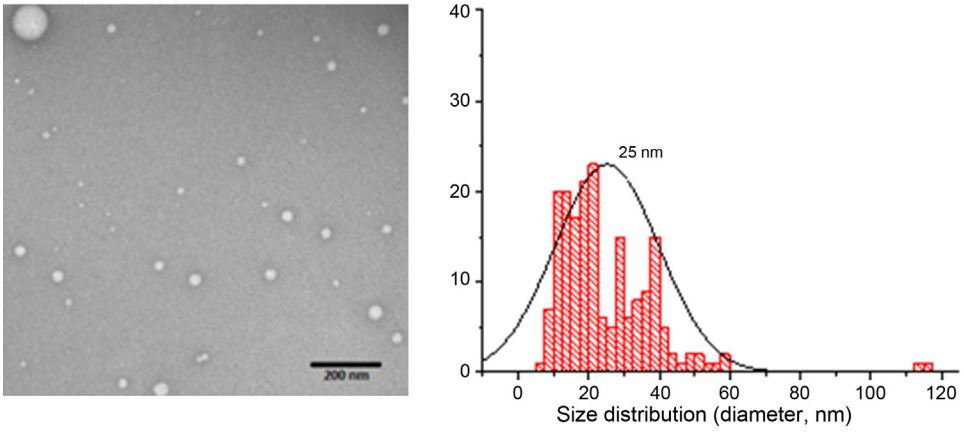

Fig. 6. Transmission electron micrograph with size distribution of XGO-*b*-XGO,Ac micelles (3 mg mL^{-1}).

Table 1
Effect of different surfactants and concentrations on the size and polydispersity index of gliadin and zein nanoparticles.

Protein	Surfactant concentration	Nanoparticle size (nm) ± SD	PDI ± SD
Gliadin	Without surfactant	436.8 ± 85.5	0.68 ± 0.04
	Pluronic F68 (0.01%)	398.4 ± 30.2	0.48 ± 0.05
	Pluronic F68 (0.05%)	382.9 ± 3.8	0.52 ± 0.05
	Pluronic F68 (0.1%)	401.4 ± 17.5	0.76 ± 0.05
	XGO-*b*-XGO,Ac (0.01%)	410.4 ± 15.7	0.55 ± 0.19
	XGO-*b*-XGO,Ac (0.05%)	371.2 ± 39.9	0.51 ± 0.03
	XGO-*b*-XGO,Ac (0.1%)	306.0 ± 22.8	0.47 ± 0.01
Zein	Without surfactant	164.5 ± 2.1	0.12 ± 0.02
	Pluronic F68 (0.01%)	128.9 ± 1.3	0.12 ± 0.01
	Pluronic F68 (0.05%)	140.9 ± 2.6	0.19 ± 0.02
	Pluronic F68 (0.1%)	125.2 ± 0.6	0.28 ± 0.03
	XGO-*b*-XGO,Ac (0.01%)	200.3 ± 1.2	0.08 ± 0.01
	XGO-*b*-XGO,Ac (0.05%)	269.5 ± 4.6	0.10 ± 0.01
	XGO-*b*-XGO,Ac (0.1%)	220.6 ± 7.5	0.14 ± 0.04

of XGO-*b*-XGO,Ac induced the formation of zein nanoparticles with larger sizes compared with those stabilized by Pluronic. In Fig. 7D we observe zein particles without any stabilizer under similar conditions to the gliadin nanoparticles, where irregular nanoparticles were obtained. Zein nanoparticles with spherical and solid morphology were observed independently of the surfactant. However, a significant effect was observed in the PDI of the samples ($p < 0.05$) (Table 1), where the XGO-*b*-XGO,Ac 5 conferred a lower PDI to the zein nanoparticles, as may be seen in Fig. 7 (right) and Table 1. Nanoparticles with a bimodal distribution were observed using Pluronic as stabilizer (Fig. 7E), while a very narrow distribution was observed in zein nanoparticles with XGO-*b*-XGO,Ac 5 (Fig. 7F). Zein nanoparticles with XGO-*b*-XGO,Ac 5 showed larger sizes, indicating the ability of this carbohydrate-based amphiphilic BCO to encapsulate more protein inside the nanoparticle core.

The results of this work showed a better performance of XGO-*b*-XGOAc 5 compared to pluronic F-68 in forming size-homogeneous zein nanoparticles. With gliadin, for both surfactants, the size and morphology of the nanoparticles were unchanged. These behavior differences between gliadin and zein in stabilizing nanoparticles can be correlated to the sharp difference between the molecular sizes of the native proteins. While zein is a mixture of proteins varying in molecular weight between 17–27 kDa (Mejia, Mauer, & Hamaker, 2007), gliadin shows a molecular weight in the range between 30–74 kDa (Guilbert et al., 2002). Another explanation could be related to the surface charge difference between both globular proteins as well as to the critical complexation and unfolding

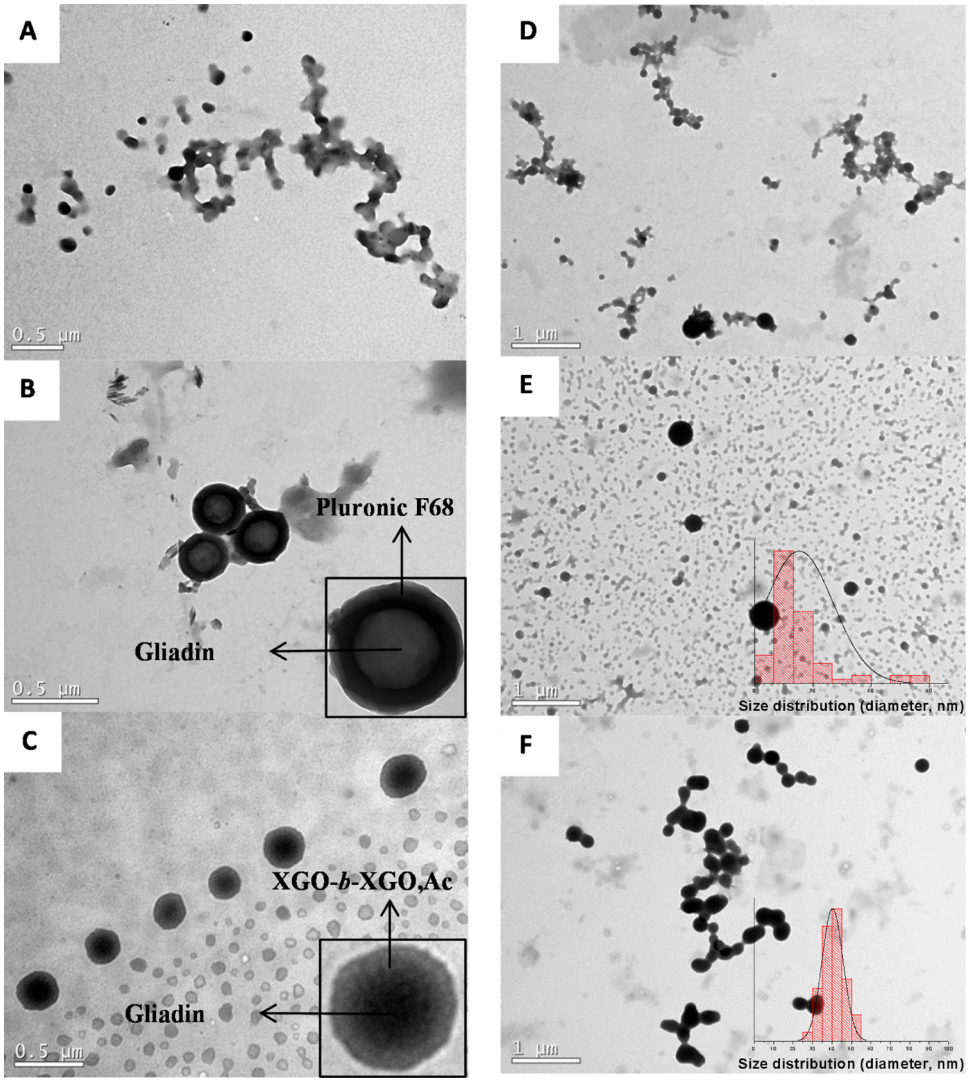

Fig. 7. Transmission electron micrograph of (left) gliadin nanoparticles (A) stabilized by 0.05% Pluronic (B), XGO-*b*-XGO,Ac (C), with magnified nanoparticles in a box and (right) zein nanoparticles (D) stabilized by 0.05% Pluronic F-68 (E) and XGO-b-XGO,Ac (F).

concentrations (Deo, Jockusch, Turro, & Somasundaran, 2003). An in-depth study will be undertaken soon.

4. Conclusions

This work reported the synthesis of a new class of amphiphilic block co-oligomer systems exclusively constituted of oligosaccharidic blocks, obtained from tamarind seeds xyloglucan. The synthetic procedure has followed the approach developed for maltoheptaose (Modolon et al., 2012), thus emphasizing its versatility. In water, the self-assembly of this XGO-based block co-oligomer led to the formation of spherical micelles with an average hydrodynamic diameter of 22 nm. Preliminary studies of the physical stability of protein (gliadin and zein) nanoparticles with the XGO-based block co-oligomer and a commercial stabilizer (Pluronic® F-68) were investigated. For protein/block co-oligomer complexes, the scattering and imaging techniques clearly identified core/shell nanoparticles where the block co-oligomer constitutes the shell protecting the inner core made from proteins. Further studies are in due course to determine the aggregation number (number of surfactant molecules involved in one micelle) by fluorescence and DLS, and the encapsulation abilities. In fact, the amphiphilic sugar-stabilized proteins could constitute an interesting biocompatible and biodegradable drug delivery system (Hawkins et al., 2008; Schmolka, 1991) or an alternative to commonly used nonionic surfactant like polysorbates (Garidel, Hoffmann, & Blume, 2009) and poloxamers (Kabanov, Lemieux, Vinogradov, & Alakhov, 2002).

Acknowledgments

We acknowledge the financial support from CNRS, CNPq and CAPES-COFECUB (project 620/08). We would also like to thank the Central Laboratory of Electron Microscopy (LCME) at UFSC and to Ismael Casagrande Bellettini for his assistance in the fluorescence analysis. The authors thank ICMG platform for analyses in mass spectrometry, C. Travelet for his help in light scattering and I. Jeacomine for technical assistance in NMR spectrometry.

Appendix A. Supplementary data

Supplementary data associated with this article can be found, in the online version, at http://dx.doi.org/10.1016/j.carbpol.2013.07.064.

References

Adair, J. H., Parette, M. P., Atinoglu, E. I., & Kester, M. (2010). Nanoparticulate alternatives for drug delivery. *ACS Nano*, *4*, 4967–4970.
Allen, C., Maysinger, D., & Eisenberg, A. (1999). Nano-engineering block copolymer aggregates for drug delivery. *Colloids and Surfaces B: Biointerfaces*, *16*, 3–27.
Ambade, A. V., Savariar, E. N., & Thayumanavan, S. (2005). Dendrimetric micelles for controlled drug release and targeted delivery. *Molecular Pharmaceutics*, *2*, 264–272.
Arangoa, M. A., Ponchel, G., Orecchioni, A. M., Renedo, M. J., Duchêne, D., & Irache, J. M. (2000). Bioadhesive potential of gliadin nanoparticulate systems. *European Journal of Pharmaceutical Sciences*, *11*, 333–341.
Arangoa, M. A., Campanero, M. A., & Irache, J. M. (2004). Potencial bioadhesivo de las nanopartículas de gliadina en el estómago. *Revista colombiana de ciencias químico farmacéuticas*, *33*, 38–47.
Barsett, H., Ebringerová, A., Harding, S. E., Heinze, T., Hromádková, Z., Muzzarelli, C., et al. (2005). Polysaccharides I. In H. Thomas (Ed.), *Advances in Polymer Science (186) Structure Characterisation and Use*. Berlin, Heidelberg: Springer.
Carpita, N. C., & Gibeaut, D. M. (1993). Structural models of primary cell walls in flowering plants: Consistency of molecular structure with the physical properties of the walls during growth. *Plant Journal*, *3*, 1–30.
Dalpathado, D. S., Jiang, H., Kater, M. A., & Desaire, H. (2005). Reductive amination of carbohydrates using $NaBH(OAc)_3$. *Analytical and Bioanalytical Chemistry*, *381*, 1130–1137.
Deo, N., Jockusch, S., Turro, N. J., & Somasundaran, P. (2003). Surfactant interactions with Zein protein. *Langmuir*, *19*, 5083–5088.
Dong, J., Sun, Q. Sh., & Wang, J. Y. (2004). Basic study of corn protein, zein, as a biomaterial in tissue engineering, surface morphology and biocompatibility. *Biomaterials*, *25*, 4691–4697.
Duclairoir, C., Nakache, E., Marchais, H., & Orecchioni, A.-M. (1998). Formation of gliadin nanoparticles: Influence of the solubility parameter. *Colloid and Polymer Science*, *276*, 321–327.
Efthymiou, T. C., Huynh, V., Oentoro, J., Peel, B., & Desaulniers, J.-P. (2012). Efficient synthesis and cell-based silencing activity of siRNAS that contain triazole backbone linkages. *Bioorganic & Medicinal Chemistry Letters*, *22*, 1722–1726.
Ezpeleta, I., Irache, J. M., Stainmesse, S., Chabenat, C., Gueguen, J., Popineau, Y., et al. (1996). Gliadin nanoparticles for the controlled release of all-trans-retinoic acid. *International Journal of Pharmaceutics*, *131*, 191–200.
Ezpeleta, I., Arangoa, M. A., Irache, J. M., Stainmesse, S., Chabenat, C., Popineau, Y., et al. (1999). Preparation of *Ulex europaeus* lectin-gliadin nanoparticle conjugates and their interaction with gastrointestinal mucus. *International Journal of Pharmaceutics*, *191*, 25–32.
Garidel, P., Hoffmann, C., & Blume, A. (2009). A thermodynamic analysis of the binding interaction between polysorbate 20 and 80 with human serum albumins and immunoglobulins: A contribution to understand colloidal protein stabilisation. *Biophysical Chemistry*, *143*, 70–78.
Greffe, L., Bessueille, L., Bulone, V., & Brumer, H. (2005). Synthesis, preliminary characterization and application of novel surfactants from highly branched xyloglucan oligosaccharides. *Glycobiology*, *15*, 437–445.
Guilbert, S., Gontard, N., Morel, M. H., Chalier, P., Micard, V., & Redl, A. (2002). Formation and properties of wheat gluten films and coatings. In A. Gennadios (Ed.), *Protein-based films and coatings* (pp. 69–122). Boca Raton, FL: CRC Press.
Halila, S., Manguian, M., Fort, S., Cottaz, S., Hamaide, T., Fleury, E., et al. (2008). Synthesis of well-defined glyco-polyorganosiloxanes by "click" chemistry and their surfactant properties. *Macromolecular Chemistry and Physics*, *209*, 1282–1290.
Hawkins, M. J., Soon-Shiong, P., & Desai, N. (2008). Protein nanoparticles as drug carriers in clinical medicine. *Advanced Drug Delivery Reviews*, *60*, 876–885.
Hisamatsu, M. J., York, W. S., Darvill, A. G., & Albersheim, P. (1992). Characterization of seven xyloglucan oligosaccharides containing from seventeen to twenty glycosyl residues. *Carbohydrate Research*, *227*, 45–71.
Jahanshahi, M., & Babaei, Z. (2008). Protein nanoparticle: A unique system as drug delivery vehicles. *African Journal of Biotechnology*, *7*, 4926–4934.
Kabanov, A. V., Lemieux, P., Vinogradov, S., & Alakhov, V. (2002). Pluronic block copolymers: Novel functional molecules for gene therapy. *Advanced Drug Delivery Reviews*, *54*, 223–233.
Kataoka, K., Harada, A., & Nagasaki, Y. (2001). Block copolymer micelles for drug delivery: Design, characterization and biological significance. *Advanced Drug Delivery Reviews*, *47*, 113–131.
Kida, T., Kajihara, K., Isogawa, K., Zhang, W., Nakatsuji, Y., Ikeda, I., et al. (2004). Sugar-amide surfactant micelles as effective reaction fields for enantioselective hydrolysis of α-amino acid esters. *Langmuir*, *20*, 8504–8509.
Kwon, G. S., Naito, M., Yokoyama, M., Okano, T., Sakurai, Y., & Kataoja, K. (1993). Micelles based on AB block copolymers of poly(ethylene oxide) and poly(β-benzyl-L-aspartate). *Langmuir*, *9*, 945–949.
Leader, B., Baca, Q. J., & Golan, D. E. (2008). Protein therapeutics: A summary and pharmacological classification. *Nature Reviews: Drug Discovery*, *7*, 21–39.
Lee, H. J., McAuley, A., Schilke, K. F., & McGuire, J. (2011). Molecular origins of surfactant-mediated stabilization of protein drugs. *Advanced Drug Delivery Reviews*, *63*, 1160–1171.
Liu, X., Sun, Q., Wang, H., Zhang, L., & Wang, J. (2005). Microspheres of corn protein, zein, for an ivermectin drug delivery system. *Biomaterials*, *26*, 109–115.
Magnusson, G., Olsson, T., & Nyberg, J.-A. (1986). Toxicity of pluronic-F68. *Toxicology Letters*, *30*, 203–207.
Mastromatteo, M., Barbuzzi, G., Conte, A., & Del Nobile, M. A. (2009). Controlled release of thymol from zein based film. *Innovative Food Science and Emerging Technologies*, *10*, 222–227.
Mejia, C. D., Mauer, L. J., & Hamaker, B. R. (2007). Similarities and differences in secondary structure of viscoelastic polymers of maize α-zein and wheat gluten proteins. *Journal of Cereal Science*, *45*, 353–359.
Modolon, S. M., Otsuka, I., Fort, S., Minatti, E., Borsali, R., & Halila, S. (2012). Sweet block copolymer nanoparticles: Preparation and self-assembly of fully oligosaccharide-based amphiphile. *Biomacromolecules*, *13*, 1129–1135.
Nakashima, K., Anzai, T., & Fujimoto, Y. (1994). Fluorescence studies on the properties of a pluronic F68 micelle. *Langmuir*, *10*, 658–661.
Nowicki, J., Sokolowski, A., & Reksa, D. (2011). Synthesis and surface active properties of novel carbohydrate-based cationic surfactants. *Journal of Surfactants and Detergents*, *14*, 179–184.
Parris, N., Cooke, P. H., & Hicks, K. B. (2005). Encapsulation of essential oils in zein nanospherical particles. *Journal of Agricultural and Food Chemistry*, *53*, 4788–4792.
Rostovtsev, V. V., Green, L. G., Fokin, V. V., & Sharpless, K. B. (2002). A stepwise Huisgen cycloaddition process: Copper(I)-catalyzed regioselective ligation of azides and terminal alkynes. *Angewandte Chemie International Edition*, *41*, 2596–2599.
Schafer, V., Briesen, H., Andreesen, R., Steffan, A. M., Royer, C., Troster, S., et al. (1992). Phagocytosis of nanoparticles by human immunodeficiency virus (HIV)-infected macrophages: A possibility for antiviral drug targeting. *Pharmaceutical Research*, *9*, 541–546.
Schmolka, I. R. (1991). Polyoxamers in the pharmaceutical industry. In P. J. Tarcha (Ed.), *Polymers for Controlled Drug Delivery (Chapter 10)*. CRC Press: Boston.
Tadros, T. F. (2005). *Applied Surfactants: Principles and Applications*. Wokingham: Wiley–VCH Verlang GmbH & Co. KGaA.

Tornoe, C. W., Christensen, C., & Meldal, M. (2002). Peptidotriazoles on solid phase: [1,2,3]-triazoles by regiospecific copper(I)-catalyzed 1,3 dipolar cycloadditions of terminal alkynes to azides. *Journal of Organic Chemistry*, *67*, 3057–3064.

Torres-Giner, S., Gimenez, E., & Lagaron, J. M. (2008). Characterization of the morphology and thermal properties of zein prolamine nanostructures obtained by electrospinning. *Food Hydrocolloids*, *22*, 601–614.

Wang, H. J., Lin, Z. X., Liu, X. M., Sheng, S. Y., & Wang, J. Y. (2005). Heparin-loaded zein microsphere film and hemocompatibility. *Journal of Controlled Release*, *105*, 120–131.

Wang, H. J., Gong, S. J., Lin, Z. X., Fu, J. X., Xue, S. T., Huang, J. C., et al. (2007). In vivo biocompatibility and mechanical properties of porous zein scaffolds. *Biomaterials*, *20*, 3952–3964.

Yadav, S. C., Kumari, A., & Yadav, R. (2011). Development of peptide and protein nanotherapeutics by nanoencapsulation and nanobioconjugation. *Peptides*, *32*, 173–187.

Zhang, R., Zhang, L., & Somasundaran, P. J. (2004). Study of mixtures of n-dodecyl-β-D-maltoside with anionic, cationic, and nonionic surfactant in aqueous solutions using surface tension and fluorescence techniques. *Journal of Colloid Interface Science*, *278*, 453–460.

Zhong, Q., & Jin, M. (2009a). Nanoscalar structures of spray-dried zein microcapsules and in vitro release kinetics of the encapsulated lysozyme as affected by formulations. *Journal of Agricultural and Food Chemistry*, *57*, 3886–3894.

Zhong, Q., & Jin, M. (2009b). Zein nanoparticles produced by liquid-liquid dispersion. *Food Hydrocolloids*, *23*, 2380–2387.

Ziegler, F. E., Fowler, K. W., Rodgers, W. B., & Wester, R. T. (1987). Ambient-temperature Ullman reaction: 4,5,4′,5′-tetramethoxy-1,1′-biphenyl-2,2′-dicarboxaldehyde. *Organic Syntheses*, *65*, 108.